Powder Technology 410 (2022) 117871

Contents lists available at ScienceDirect

Powder Technology

journal homepage: www.journals.elsevier.com/powder-technology

Multivariate correlation of PolyArylEtherKetone powder properties for additive manufacturing and a method for predicting spreading in polymer powder bed fusion

Richard Davies *, Ken Evans, Oana Ghita

University of Exeter, College of Engineering, Mathematics and Physical Sciences, Harrison Building, Streatham Campus, North Park Road, EX4 4QF Exeter, UK

HIGHLIGHTS

- Bulk and dynamic flow properties are captured with a Universal Powder Rheometer.
- Multivariate Correlation interprets linear relationships between properties.
- Key relationships between PSD, Circularity and Powder Rheology are identified.
- Normalised Aeration Sensitivity used to predict spreading.

GRAPHICAL ABSTRACT

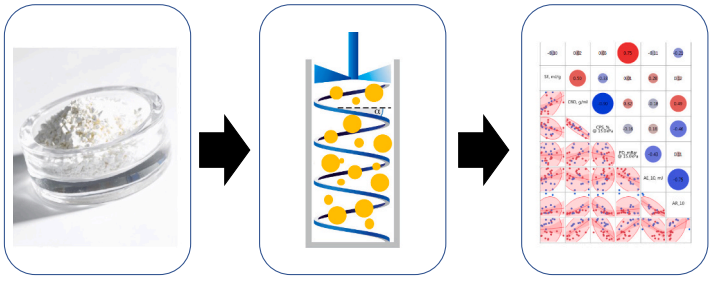

ARTICLE INFO

Keywords:
Laser powder bed fusion
Polyaryletherketone
Universal powder rheometer
Particle size distribution
Multivariate correlation

ABSTRACT

In a study of unique scale, twenty-four milled Polyaryletherketone (PAEK) polymer powders produced during the development of new grades for Powder Bed Fusion (PBF) were tested using a universal powder rheometer and particle size and shape analyser. Multivariate correlation was used to identify the linear relationships between bulk and dynamic properties and particle size. The flow energy, which measures the energy required to displace powder when in a loosely packed state, was found to have very strong relationships with both the powder density and its compressibility, and both the density and compressibility share a very strong relationship with each other. Partition modelling determined that normalised aeration sensitivity (NAS) was the key indicator when predicting powder spreading. The study highlights the importance for complete and pertinent datasets to allow the development of accurate correlations and the need to capture the PBF spreading performance when developing materials for additive manufacturing.

1. Introduction

Powder Bed Fusion (PBF) of polymers is one of the most important methods of Additive Manufacturing (AM) whereby parts are created in three dimensions from sliced Computer Aided Design (CAD) data layer upon layer. The most common polymer currently used in PBF is

* Corresponding author.
E-mail address: richard.davies@exeter.ac.uk (R. Davies).

https://doi.org/10.1016/j.powtec.2022.117871
Received 20 May 2022; Received in revised form 12 July 2022; Accepted 19 August 2022
Available online 22 August 2022

Polyamide 12 (PA12) but recently new polymers have been commercialised for use with PBF. Polyamide 11, Polyetherketone (PEK), Polyetherketoneketone (PEKK), polypropylene and thermoplastics polyurethanes (TPUs) have all been commercialised and are available in grades suitable for powder bed processes, as reported by Stansbury and Idacavage [1].

The requirements for a polymer's suitability for PBF are multifaceted [2], including thermal and rheological properties, crystallisation behaviour and most critical, the ability to form a fine powder that can spread smoothly in fine layers of 100-120 μm thickness without agglomeration.

Depending on the chemical structure of the polymer, there are several methods of forming fine powders suitable for PBF machines, typically a powder with a median particle diameter of 50-60 μm. The most common PBF grade polymer, PA12 can be formed via precipitation or direct polymerisation and these powders contain particles that are well-rounded [3] and have excellent flow properties. Polystyrene powders containing spherical particles have been shown to flow and spread with excellent results yet are less common in industrial PFB usage due to poor mechanical performance [4] and the requirement for post processing such as resin infiltration [5]. Methods of producing near spherical polymer particles for the PBF process have also been proved at laboratory scale. Wang et al., [6] formed PA12 microspheres by blending PA12 powder in formic acid with Polyvinylpyrrolidone (PVP-K30) acting as a dispersal agent, then filtering and drying the resulting particles. Solution dispersion of Polyamide 6 (PA6) and three different nano-additives was explored by Wahab et al., [7] to enable spray drying of a PA6 composite spherical fine powder. Formic acid was again used to dissolve the PA6 into a solution. Wang et al., [8] used thermally induced phase separation to create a Polyetheretherketone (PEEK) composite fine powder. 20 wt% Phenyl Sulfone at a temperature of 200 °C was used to dissolve the PEEK before precipitation. Composite particles have been produced by exploiting immiscibility of certain polymers in specific solvents. Chen et al., [9] fabricated Polyetherimide/Polyetheretherketone (PEI/PEEK) powders containing graphene nanoplatelets (GNPs) by dissolving PEI in Dichloromethane and adding PEEK powder before drying. The resulting powder consisted of milled PEEK particles coated in PEI/GNP. Many of these processes presented above have limited ability to scale up or be delivered in a continuous process. For large scale production of fine powders, milling is an established process that is economically attractive and proven to be able to produce fine powders of a particle size range suitable for the PBF process. However, the resulting morphology and flow properties can be undesirable [10]. The type of milling process can also affect the morphology of the resulting powders as reported by Chen et al., [11].

Powder flow can be characterised by multiple methods [12] which fall into two main categories: tests which produce a single value such as Angle of Repose, or tests which produce multiple values such as Jenicke's Shear test [13] (see Table 1). Leturia et al., [14] and Tay et al., [15] concluded it is desirable to use a characterisation method which mimics the application, yet powder flow cannot be accurately quantified with a single indicator.

Many of the studies discussed below have used selective values obtained from a powder rheometer, or a combination of tests (single or multi value test) to evaluate changes in powder properties. More widely published is the use of powder rheometers for other polymer and metal powders and their suitability for AM. The rheology data gathered through the Freeman FT4 technology collects ten powder parameter values across four standard test methods: i) stability and variable flow, ii) aeration, iii) compressibility, iv) permeability for a single type of powder with different flow characteristics. The stability and variable flow tests record the Basic Flow Energy (BFE), Stability Index (SI), Flow Rate Index (FRI), Specific Energy (SE) and Conditioned Bulk Density (CBD). The Aeration test records Aeration Energy (AE), Aeration Ration (AR) and the Normalised Aeration Sensitivity (NAS). The compressibility and permeability tests record Compressibility (CPS) and Pressure Drop (PD) respectively.

Table 1
Classification of powder tests based on the results given: single value or multi-value results. [12].

Single value tests	Hausner Ratio [tap consolidation], Angle of Repose, Funnel Flow, Imse Test, Carr Flowability Index, Compression
Multi value tests	Rotary Drum Test, Powder Rheometer Test, Warren Spring Bradford Cohesion Test, Shear Test

There are only a few publications specifically studying PAEK powder flow characteristics with a universal powder rheometer for the application of high temperature PBF. Yazdani, et al., [16] used four rheometer values [17] (BFE, SE, SI and FRI) to describe changes between the fine powders EOS HP3 PEK, Victrex PEEK 450PF and C-coated Inorganic Fullerene-like WS2 coated PEEK 450PF and Graphene Nanoplatelet coated PEEK 450PF. The purpose of the powder analysis was to ascertain whether the new developed powder will have good flow characteristics for use in the PBF process. No significant changes in the stability of the composite powders compared to the plain PEEK were observed, but a noticeable change in the sensitivity to flow rate as measured by FRI. The authors concluded the nano-composite powders had improved flow over the plain PEEK powder, comparable to the HP3 PEK yet the focus of the study was the preparation of a coated powder suitable for the PBF process. The Particle Size Distribution data of the powders was presented comparing the original powder to the new composite powders, but no conclusions were presented as to the interactions between size distribution and flow characteristics.

Chen et al., [18] recorded the changes in rheometer outputs (BFE, SE, CBD and SI) of EOS PA2200 (PA12), PVA coated PA12, 0.1% and 0.5% Graphene Nano Platelet PVA coated PA12. The coating of PVA reduced both the BFE and the SE without significant effect on the CBD and SI, and the addition of GNP to the PVA coating further reduced the BFE and SE. The study did not make any conclusions on flow properties of the composite powders but commented on the lack of change before and after the coating process and therefore the suitability of the process as an addition to the PA powder for use within the PBF process.

In a separate study Chen et al., [19] presented variations in BFE, SE, CBD and SI of PEK and PEK Carbon Fibre composite powders for the use in high temperature PBF. The variation in the data was discussed but not linked with the findings from the particle size or fibre content.

In a study of 12 powders, including PA12, Stainless Steel, Titanium, Gypsum and various grades of Aluminium Oxide, Tan et al., [20] combined Particle Size Distribution, Particle Sphericity and powder rheometer test values – CPS, FRI, SE and Shear values into a unique and non-standard Comprehensive Evaluation Index (CEI) using Principal Component Analysis and quantified flowability from the avalanche angle measured in front of the spreading mechanism of a self-built powder spreading rig. This CEI value was found to have a strong relationship with the avalanche angle of the powders. They concluded that the shear indexes, FRI sensitivity and SE have the greatest influence on the CEI, and that the sphericity is not a critical requirement for good flow. Yet, there was little discussion on the selection process of this combination of single and multi-value tests.

Ziegelmeier et al., [21] combined single and multi-value testing, the Hausner Ratio (HR) with several FT4 powder rheometer values (BFE, SE, CBD), and Avalanche Angle and Density from a Rotary Powder Analyser (RPA). They compared three grades of cryogenically milled TPU powders, distinct by their PSD against EOS PA2200 (PA12) in order to gauge suitability for the PBF process, however final testing in the process to validate the results was not reported. The conclusions focused on the avalanche angle obtained from a rotary powder analyser as a reliable and reproducible measure of cohesion. BFE is also an accurate method yet unable to distinguish between powders of significantly different morphologies. The Avalanche Angle again was chosen as the preferred method to measure flowability, and the Hausner Ratio the preferred

method for measuring packing efficiency. Although size and shape (sphericity and width/length ratio) data was presented, no conclusions were made in relation to the dynamic flow data. In a study of initial spreading of three grades of gas atomised Al-10Si-0.5 Mg powder, Snow et al., [22] presented SE and FRI in combination with: i) flow time, apparent density, tapped density and angle of repose from a Hall Flowmeter, ii) avalanche average, energy average and angle average from a Revolution powder analyser, iii) percentage of powder coverage, powder deposition rate, time averaged avalanche angle and rate of change of avalanche angle from a self-built powder spreading rig.

The values gathered from the powder spreading rig were proposed as new metrics to quantify spreadability, although the experimental method was limited to the initial spreading of powder over a substrate yet the PBF process involves spreading of powder over a multitude of previously deposited layers. They concluded a powder's angle of repose can be used to predict the spreading performance as quantified by the values from the spreading rig.

Another example where powder rheometer values were selectively chosen (BFE, SI and SE) was in the development of a milled PA11 composite powders for use in a Farsoon HT251P PBF system with a roller spreading mechanism (Jin et al., [23]). The authors draw conclusions on the powder flow characteristics from just the BFE, SI and SE values, yet the data is insufficient to make such a conclusion as no information regarding the bulk density or packing is presented.

This study will focus on characterisation of twenty-four grades of milled PAEK powders for use in the PBF process and draw key correlations between the measured bulk flow properties and particle size distribution values using multivariate correlation, and identify which values are significant when testing spreadability.

2. Experimental methods

2.1. Materials

Twenty-four grades of milled, PAEK powders were supplied by Victrex [24] including PEEK, PEK and PEEK-PEDEK copolymer grades. PEEK-PEDEK grades are referred to as PDK in the rest of the paper. Eleven of the powders underwent a thermal treatment to improve flow prior to testing as outlined by Muller et al., [25]. The powders were investigated in their pure, as milled form with no additional flow additives.

2.2. Particle size distribution

Particle size and distribution was measured using a Microtrac Sync [26] dry powder analyser by means of tri laser diffraction [27]. Data gathering was performed using FLEX 12.0.0.0 software. The dry powder sample was vacuum gathered by the sample collection tube to form a well dispersed stream of particles into the sample cell. Sample dispersion was set at 5 psi and the test repeated three times for each powder sample. The average values of the three repeat tests were recorded. The D50, D90 and D10 values were reported, and the span of the distribution. The D50 represents the particle size of which 50% of the distribution falls below, and similarly D90 and D10 represent 90% and 10% of the distribution. The span of the distribution, S was calculated by the following equation.

$$S = \frac{D90 - D10}{D50}$$

Equation 1. Span of a volume based distribution.

2.3. Particle shape analysis

Particle Shape parameters were captured simultaneously with the PSD values from the Microtrac Sync by means of Dynamic Image Analysis using a high speed camera and stroboscopic LED illumination. The images analysis was performed using FLEX 12.0.0.0 software.

To evaluate the particle shape characteristics, the distribution mean circularity of the sample, from each of the three repeat tests was averaged and reported as a single value for each different PAEK powder. The circularity, which is known to affect spreading [4] was selected to evaluate the roundness of the particles and was calculated by Eq. 2, where C is the circularity, A is the particle area and p is the perimeter, as defined by ISO 9276-6. The circularity value is dimensionless and ranges from 0 to 1 where 1 is a perfect circle.

$$C = \sqrt{\frac{4\pi A}{p^2}}$$

Equation 2. Circularity of a particle.

2.4. Powder rheology

Bulk powder flow properties were measured at room temperature using a universal powder rheometer [17]. Ten values were measured for each powder sample across four separate tests as described below and repeated three times. The universal powder rheometer uses a twisted blade moving through the powder sample in a vessel of a known volume. (See Fig. 1) The sample volume is established by splitting the top of the vessel after the conditioning cycle of the test and the sample can be aerated by passing air through a perforated base, or the blade can be switched to a vented piston for measuring compressibility or permeability. The flow energy (fE) is calculated from the blade radius (r), the helix angle (α), the torque (T), the axial force on the blade (F) and the change in height of the blade (dH)

$$fE\ (mJ) = \sum \left[\left(\frac{T}{R tan(\alpha)} + \mathrm{F} \right) \mathrm{d}H \right]$$

Equation 3. Flow energy measurement from the blade as it travels through the sample [28].

Four test methods were used to characterise the powders.

1) Stability and Variable Flow Test: The stability and variable flow test measured the testing of a pre-conditioned fixed volume of powder. The powder rheometer measured the height of the powder blade, the torque of the blade, and the force applied on the sample through a load cell in the base. The sample hysteresis of the operator loading the powder sample was removed by way of a conditioning stage at the start of the test, then seven energy tests were performed with a blade tip speed of 100 mm/s, with an additional four energy tests at a reducing blade tip speed of 100, 70, 40 and 10 mm/s respectively, and the following measurements were obtained: Basic Flow Energy (BFE), (mJ), Stability Index (SI) Flow Rate Index (FRI), Specific Energy (SE) (mJ/g) and Conditioned Bulk Density (CBD) (g/ml).

1) Basic Flow Energy (BFE), *Energy Test 7* (mJ)
2) Stability Index (SI), (*Energy Test 7*)/(*Energy Test 1*)
3) Flow Rate Index (FRI), (*Energy Test 11*)/(*Energy Test 8*)
4) Specific Energy (SE), ((*Up Energy Cycle 6* + *Up Energy Cycle 7*)/2)/(*Split Mass*) (mJ/g)
5) Conditioned Bulk Density (CBD), (*Split Mass*)/(*Split Volume*) (g/ml)

2) Aeration Test: The aeration test measured the energy required to move the sample as a function of increasing air flow, from 0 to 10 mm/s through the powder. As the air flow increases, most powders began to fluidise to some degree, and the following measurements were obtained: Aerated Energy (AE) (mJ), Aeration Ratio (AR) and Normalised Aeration Sensitivity (NAS).

Due to the cohesive nature of the milled PAEK powders, a modified Aeration Test method with a helix angle of 40° was used to obtain valid test data, avoiding powder lifting during the test sequence.

1) Aerated Energy (AE), *Energy* (*Air Velocity* 10 *mm/s*) (mJ)

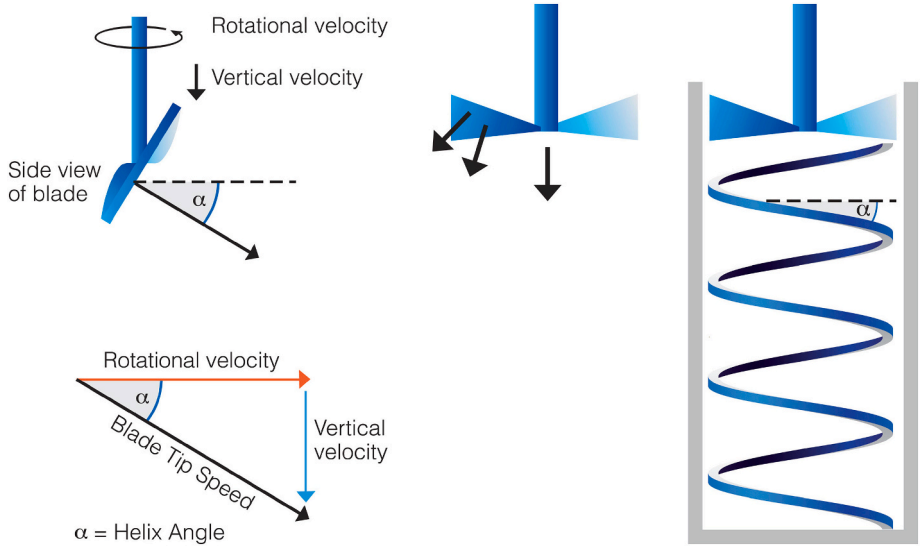

Fig. 1. Illustration of the principles of the universal powder rheometer showing (left) the helix angle α and (right) the path of the blade and the force direction. (Images courtesy of Freeman Technology 2022).

2) Aeration Ratio (AR), *Energy* (*Air Velocity* 0*mm/s*)/*Energy*(*Air Velocity* 10*mm/s*)
3) Normalised Aeration Sensitivity (NAS), *Δ*(*Normalised Energy*)/*Δ*(*Air Velocity*) (s/mm)

3) Compressibility Test: The compressibility test measured the ability of the powder to compress as a function of applied normal stress and is expressed as the percentage change in volume (%). The vented piston was used to apply force to the pre-conditioned powder sample after splitting the vessel to establish a starting fixed volume.

4) Permeability Test: The permeability test measured the ability of the powder to transmit a fluid (air) through its bulk by means of a vented base in the measuring split vessel and a vented piston, where the sample is compressed at varying forces with a constant air velocity passed through the sample. The pressure drop (PD) across the powder bed was measured for each applied normal stress and the final PD at 15 kPa recorded as per the standard methodology for permeability (Freeman Technology, 2009).

The limitation of the Freeman FT4 is that the samples can only be tested at a maximum temperature of 40 °C, whereas the PBF process for PAEK is undertaken between 290 °C to 370 °C.

2.5. Spreading trials

Samples of each of the powders were manually loaded into an EOS P 800 fitted with a dual set of compression blades for powder spreading. The build chamber baseplate was positioned at a default 5 mm from the recoating blades and the recoater mechanism moved across the build area at a speed of 200 mm/s. The sample was heated to 250 °C using the internal infrared heaters and the chamber heater. The build plate was lowered by 120 μm and a fresh layer of powder was applied. The cycle was repeated ten times. After the tenth cycle, the sample was allowed to cool to room temperature and the surface was visually assessed for smooth spreading without agglomeration and assigned a Pass or Fail response. (See Fig. 2)

2.6. Multivariate correlation

JMP v15 data analysis software [29] was used to analyse the results of the powder rheometer and the particle size distribution. Multivariate correlation was first used to determine the linear relationships between the ten mean values obtained from the rheometer with respect to each other and then the linear relationships of the rheometer data with the particle size distribution. The correlations are estimated by Row-wise method which calculates the Pearson Product-Moment Correlation to measure the strength of the linear relationship, r between two variables by the following equation.

Fig. 2. Image of spreading trial fail result for PDK12 (left) and PDK12-T pass result (right).

$$r = \frac{\sum (x-\bar{x})(y-\bar{y})}{\sqrt{\sum (x-\bar{x})^2}\sqrt{\sum (y-\bar{y})^2}}$$

Equation 4. Pearson Product-Moment Correlation.

The strength of the relationship is measured with the correlation coefficient which can range from −1 to +1 where 0 exhibits no correlation [29].

2.7. Partition model

The output of the Spreading Trial is a categorical value (pass or fail) whilst the powder rheometer values, the PSD and the shape values are continuous. For this reason an alternative method to the Multivariate Correlation was chosen. The Partition function within JMP creates a decision tree model that identifies the most important factors in predicting the categorical response [29]. The data is recursively partitioned or split according to the relationship between the predictor and the response value. The function chooses the optimum number of splits from a large number of possible splits.

3. Results and discussion

To establish the repeatability of the values recorded, the stability and variable flow test was repeated ten times for separate samples of a grade of a randomly selected PDK powder. The values presented in Table 2 show excellent repeatability for the ten individual samples, and thus the further testing across all new samples was reduced to three repeats, with the mean value used for each test. The samples used in the repeatability test were not used in Table 3, a new set of data of three repeats was recorded.

The mean values for each of the powder grades are presented below in Table 3. Samples which underwent thermal treatment referred to in section 2.1 are denoted as Sample-T. The thermally treated powders had flow and spreading characteristics which were suitable for processing in an EOS P 800 high temperature PBF system and mechanical test specimens were successfully manufactured [30], however mechanical data is not part of this study.

The particle size distribution, circularity and spreading result of each of the samples is presented below in Table 4. Mean values are of three repeat tests which were calculated for each powder.

The characterisation tests were performed at room temperature due to the technical limitations of the Freeman FT4 and the Microtrac Sync. Only the spreading trial was performed at a temperature close to the PBF process. It is expected that temperatures above the glass transition of the polymer would impact on the bulk solid flow properties [31]. In order to perform characterisation of the bulk solid at high temperatures, bespoke equipment such as the High Temperature Annular Shear Cell proposed by Tomasetta et al., [32] and researched by Ruggi et al., [33] or the Anton Paar MCR [34] would be required. It would be desirable to gather similar PAEK flow properties at elevated temperatures.

Table 2
Ten repeat results of the PDK11 powder grade.

Test Number	BFE, mJ	SI	FRI	SE, mJ/g	CBD, g/ml
Powder Test 1	93.67	1.01	1.57	5.25	0.29
Powder Test 2	89.52	0.97	1.57	5.17	0.29
Powder Test 3	88.11	1.00	1.58	5.16	0.29
Powder Test 4	88.31	0.99	1.51	5.14	0.29
Powder Test 5	89.32	0.97	1.57	5.16	0.30
Powder Test 6	90.04	1.00	1.61	5.23	0.29
Powder Test 7	96.59	0.99	1.64	5.30	0.29
Powder Test 8	93.75	0.97	1.62	5.18	0.29
Powder Test 9	88.91	0.98	1.57	5.25	0.29
Powder Test 10	89.63	0.96	1.57	5.16	0.29
Mean	90.79	0.98	1.58	5.20	0.29
Standard Deviation	2.85	0.02	0.04	0.06	0.00

3.1. Multivariate correlation of rheometer values

The results of the multivariate correlation analysis are presented as a matrix in Fig. 3. The upper right section displays the correlation value *r* between pairs of variables, also visualised as significance circles of different sizes where a larger circle indicates a stronger relationship between the paired variables. A strong positive relationship, where an increase in a variable results in an increase in another variable, is visualised as a large red significance circle. Negative relationships, where an increase in a variable leads to a decrease in another variable, are visualised in blue. The lower left section mirrors the results in the upper right section, and displays the individual points, the regression line with 95% level confidence curves, and the 95% density ellipses which enclose 95% of the points. The larger the significance of the relationship, the closer the individual points are to the regression line which is also represented in the 95% density ellipse closely fitting the regression line. The direction of the regression line indicates whether the correlation is positive or negative, which is also represented by the colour of the significance circles.

The correlation values are also presented in a table in the Appendix.

Similar to the correlation study by Evans [35], the absolute *r* values were categorised as strong correlations ($0.6 < r < 0.8$) and very strong correlations ($r > 0.8$).

Based on the above classification and the correlation matrix in Fig. 3, five very strong relationships and nine strong relationships were identified and are presented in Table 5.

The BFE was found to have a very strong positive linear relationship with the CBD, and a very strong negative linear relationship with the CPS. The CBD is a combination of the particle's intrinsic density and the bulk powder's ability to pack into a fixed volume. At the start of each test, a powder with a low CBD has a greater amount of entrained air between the particles which is expelled during the compression test, resulting in a higher CPS. Unlike the results of Tan et al., [20] where the BFE was found to be overly influenced by varying material densities, the PAEK samples share a similar density so the increase in CBD is more likely to be the result of improved packing.

The influence of the CPS on BFE is explained by the downwards motion of the twisted blade during the BFE measurement. Within the fixed volume of the test vessel, a powder with a high compressibility allows for compactions at the face of the blade, localising the stress transition zone and air pockets in the uncompressed powder bulk can then accommodate these particles resulting in a lower BFE for the more cohesive powder sample.

The FRI was found to have a strong positive linear relationship with the PD. The sensitivity to flow rate increases when the sample has a higher PD or is less permeable. During the test, air is flowing between the particles and acting as a lubricant. It is reasonable to conclude that at high speeds the powder has less interparticle contacts points which would allow for localised compression as discussed previously, and air is able to flow between the particles in the uncompressed region regardless of its permeability in a static state. At lower speeds the air between particles has time escape the bulk powder, resulting in more interparticle contact points and more overall compression due to consolidation and a less permeable powder state. The higher the recorded static PD the greater the difference between the flow energy at high or low speed.

The NAS has a strong positive linear relationship with both the CBD and the PD. A sample with a higher NAS fluidises more easily, and during the conditioning cycle is more readily able to consolidate resulting in a higher bulk density which is less permeable as recorded by a higher PD value.

The AE was found to have a strong negative linear relationship with the AR. As the air flow is increased throughout the test sequence, the powder begins to fluidise, reducing the measured force on the twisted blade. As previously discussed, a cohesive powder can present a lower BFE due to localised compression. During the aeration test sequence there is no air flow at the start and a low flow energy can be recorded. As

Table 3
The average rheology parameters measured for the 24 PAEK powder grades.

Material	BFE, mJ	SI	FRI	SE, mJ/g	CBD, g/ml	CPS, % @ 15.0 kPa	PD, mBar @ 15.0 kPa	AE_10, mJ	AR_10	NAS, s/mm
PDK1	52.69	1.07	1.86	5.08	0.27	24.33	1.85	9.48	4.51	0.22
PDK1-T	69.45	1.15	1.97	5.14	0.32	23.32	2.46	10.09	5.41	0.36
PEK	167.16	1.08	1.62	6.83	0.43	16.24	1.27	11.34	10.90	0.40
PDK2	118.81	0.91	2.06	6.87	0.37	21.63	1.39	15.68	7.13	0.27
PDK2-T	166.56	1.18	1.65	6.73	0.43	17.05	2.06	7.33	19.42	0.42
PDK3	55.21	0.93	1.77	5.17	0.29	25.67	1.94	10.78	5.03	0.23
PDK3-T	82.74	1.12	1.95	5.90	0.34	23.63	2.80	10.62	5.79	0.38
PDK4	179.82	0.97	1.43	6.02	0.46	14.50	1.06	16.55	10.33	0.27
PDK5	124.41	0.98	1.59	8.87	0.39	21.90	1.48	16.52	6.58	0.23
PDK6	133.95	1.14	1.65	7.74	0.39	20.11	1.88	13.41	8.32	0.28
PDK6-T	173.38	1.28	1.60	5.89	0.49	17.11	2.00	8.42	16.35	0.43
PDK7	114.76	1.38	1.32	6.24	0.29	26.13	0.66	16.99	5.68	0.18
PDK7-T	136.94	1.41	1.37	5.90	0.34	21.37	0.84	3.26	38.85	0.31
PDK8-T	174.03	1.16	1.75	7.03	0.49	17.54	2.83	3.75	36.51	0.44
PDK9	125.05	1.11	1.54	6.78	0.37	21.75	1.43	13.90	6.96	0.24
PDK9-T	137.35	1.32	1.68	7.34	0.41	21.04	2.29	7.09	16.78	0.43
PDK10	89.43	0.90	1.49	5.80	0.33	24.11	1.29	11.29	6.96	0.19
PDK10-T	141.56	1.41	1.65	6.41	0.38	20.37	1.72	13.05	6.67	0.39
PDK11	98.30	1.21	1.55	5.73	0.30	24.52	1.06	12.36	6.72	0.28
PDK11-T	87.26	1.31	1.97	5.61	0.33	24.90	2.41	10.25	6.16	0.37
PDK12	95.16	1.23	1.33	6.27	0.27	27.76	0.82	13.41	6.07	0.19
PDK12-T	101.20	1.35	1.45	5.30	0.31	22.48	1.04	7.45	13.74	0.35
PEEK	136.46	0.99	1.57	6.64	0.36	22.25	1.24	14.97	8.57	0.28
PEEK-T	154.56	1.12	1.70	6.84	0.40	22.44	1.76	12.50	10.99	0.39

Table 4
The average Particle Size Distribution, Span and Circularity values of the 24 PAEK powder grades including the outcome of the spreading trial.

Material	D90	D50	D10	Span	Circularity	Spreading response
PDK1	107.40	57.57	22.17	1.48	0.68	Fail
PDK1-T	111.20	53.48	23.11	1.65	0.69	Pass
PEK	94.32	55.70	31.64	1.13	0.71	Fail
PDK2	106.00	51.53	30.04	1.47	0.70	Fail
PDK2-T	100.70	50.83	31.16	1.37	0.71	Pass
PDK3	145.40	64.40	20.24	1.94	0.67	Fail
PDK3-T	149.90	63.82	19.92	2.04	0.68	Pass
PDK4	105.30	69.84	43.61	0.88	0.71	Fail
PDK5	184.20	50.50	29.41	3.07	0.71	Fail
PDK6	68.24	41.68	26.24	1.01	0.71	Fail
PDK6-T	85.22	45.81	27.62	1.26	0.71	Pass
PDK7	100.60	68.37	41.05	0.87	0.65	Fail
PDK7-T	95.00	66.46	42.24	0.79	0.67	Pass
PDK8-T	71.11	44.28	27.49	0.99	0.73	Pass
PDK9	78.77	51.12	31.55	0.92	0.71	Fail
PDK9-T	74.22	48.40	28.86	0.94	0.71	Pass
PDK10	87.97	56.35	27.75	1.07	0.68	Fail
PDK10-T	108.70	58.61	23.06	1.46	0.69	Pass
PDK11	128.50	70.89	31.91	1.36	0.67	Fail
PDK11-T	104.10	52.58	22.43	1.55	0.68	Pass
PDK12	98.25	66.68	40.14	0.87	0.68	Fail
PDK12-T	92.04	65.47	41.48	0.77	0.68	Pass
PEEK	100.70	59.38	32.15	1.15	0.67	Fail
PEEK-T	97.92	57.74	31.11	1.16	0.68	Pass

air flow is increased, a more cohesive powder still exhibits a higher flow energy (AE) and thus the ratio between aerated and non-aerated energy is low.

The PSD Span value was found to have a very strong positive relationship with the D90 value indicating that samples with a larger D90 particle size also had a broader distribution. The more interesting correlations were those between PSD values and rheology values, the D10 value was found to have a strong negative relationship with the PD and FRI values. As the D10 value increases, the PD value decreases. A sample with a low PD is more permeable. This indicates that a sample with a large number of small particles consolidates well to form a non-permeable bulk solid.

In the case of the FRI, as the D10 value increases, the sensitivity to flow rate decreases suggesting the absence of smaller particles during the dynamic test reduces the resistance to flow at low speeds. This may be a result of the small particles packing into the voids between larger particles at low speeds and less so at higher speeds when the bulk solid is in a more fluidised state. The FRI was reported to be one of the main influences on the CEI value proposed by Tan et al., [20] yet the PSD data was not included in the calculation of the CEI.

The influence of the D10 value on PD and FRI is important when producing a fine powder suitable for PBF, and identifies the importance of measuring the complete distribution of the fine particles when considering processes such as PBF where permeability and sensitivity to flow rate are important when controlling process parameters such as the recoating speed of the new powder layer. Commercial PBF polymer powders are often categorised by just the D50 value, which whilst informing the consumer of the typical particle size, does not provide enough information when considering the suitability for PBF.

The Circularity was found to have a very strong positive relationship with the CBD and a strong positive relationship with the BFE. Circularity was also found to have a strong negative relationship with the CPS and the D50. This indicates that powder samples with a higher mean circularity consolidate better resulting in an increased CBD which is less compressible. The relationship between CBD and BFE was discussed previously. This is in agreement with Tan et al., [20] who found powders with large spherical particles have good flowability. This would suggest that the PAEK powders with higher circularity and corresponding higher CBD with lower CPS will exhibit better flowability.

The linear relationships identified using multivariate correlation of the rheometer values are not suitable to make conclusions on powder flow performance in the PBF process as this data is not linked with continuous values measured during the spreading and recoating process, yet they are of great importance when investigating and characterising the static and dynamic properties of powders for PBF. The relationships clearly identify why statements such as low BFE indicates good flow [23] should be avoided when comparing different powders, due to the influence of CBD and CPS on the BFE, and why full testing of the powder is desirable to fully understand the characteristics of a powder.

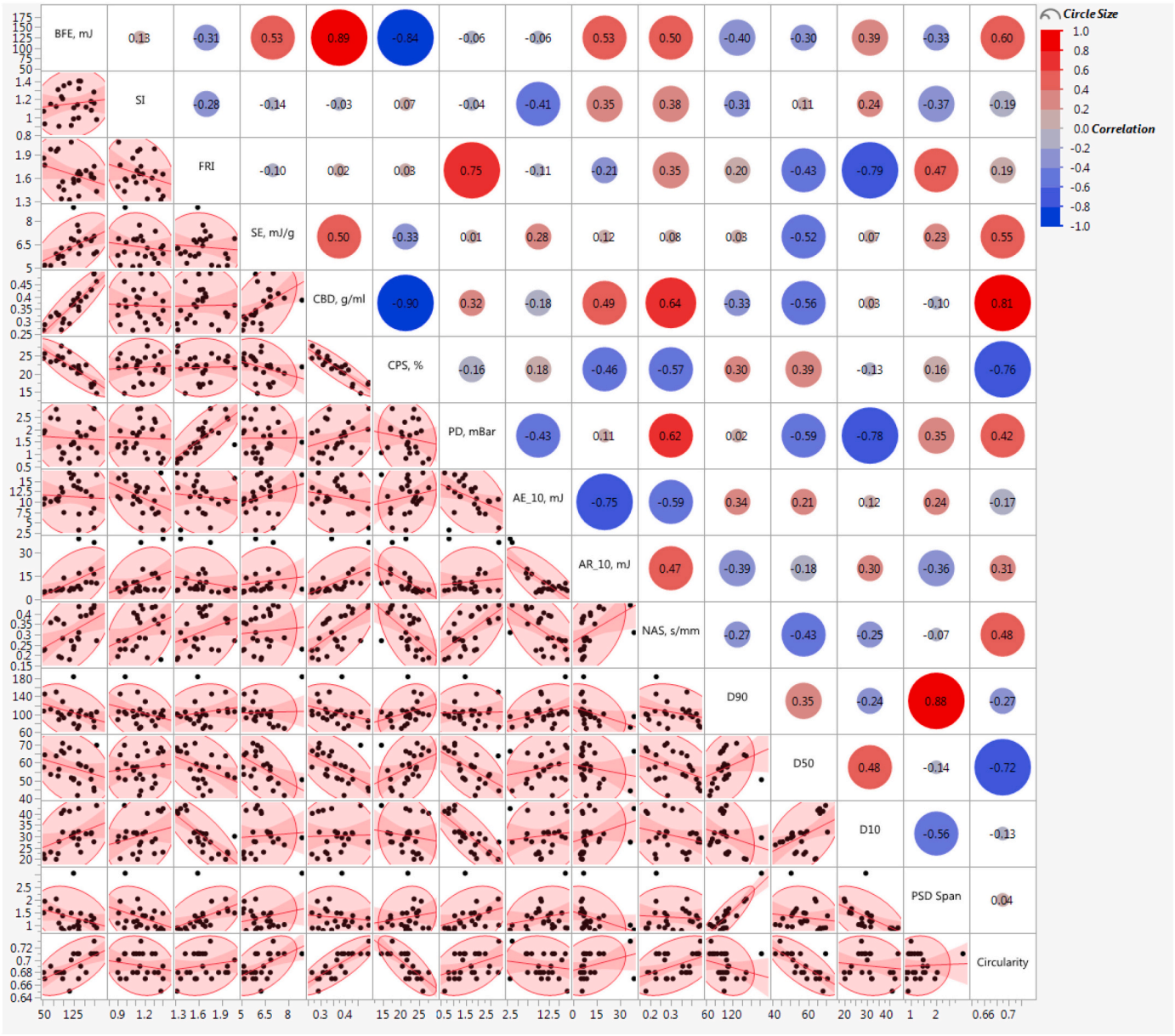

Fig. 3. Correlation matrix of the ten rheology values, the PSD and the Circularity for the twenty-four PAEK powders. The upper right side shows the part level correlation, and the lower left side shows the corresponding scatter graphs. The red circles represent a positive correlation and the blue a negative correlation. (For interpretation of the references to colour in this figure legend, the reader is referred to the web version of this article.)

Table 5
The very strong and strong relationships between powder rheology measurements, PSD and Circularity.

Very Strong correlations ($r > 0.8$)	BFE – CBD (positive)
Strong correlations ($0.6 < r < 0.8$)	CBD – CPS (negative) BFE – CPS (negative) D90 – PSD Span (positive) CBD – Circularity (positive) FRI – PD (positive) CBD – NAS (positive) PD – NAS (positive) AE – AR (negative) PD – D10 (negative) FRI – D10 (negative) BFE – Circularity (positive) CPS – Circularity (negative) D50 – Circularity (negative)

3.2. Partition model of the spreading trial

Of the twenty-four powders sampled, thirteen were randomly assigned in the model for training to estimate the model parameters, and eleven assigned for validation of the predictive ability of the model.

The Normalised Aeration Sensitivity (NAS) was found to be the most significant value from the data gathered using the Partition function when considering all the measured values and the categorical response of successful spreading in the EOS P 800. It was observed that powders with NAS of >0.31 had a response of "Pass" for spreading without agglomeration. (See Fig. 4) The RSquare for the validation is 0.9, where 1 is a perfect fit, showing the training portion of the model is robust. However the RSquare value for the validation portion of the model is only 0.505 so does not accurately fit the data. The partition tree does indicate that data gathered from the Aeration test (AE, AR, NAS) is important when considering the powders ability to spread smoothly without agglomeration. Unlike the findings of Ziegelmeier et al., [21]

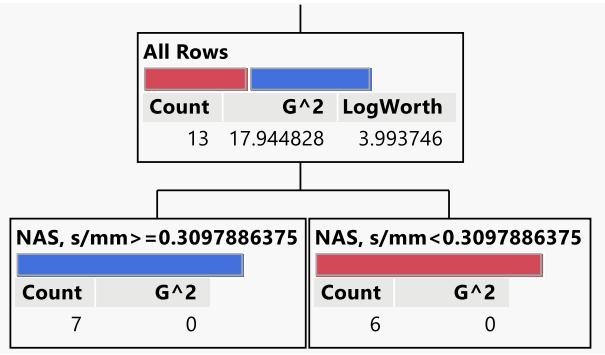

Fig. 4. The Partition Tree of the training data for the categorical response of the spreading test including the G^2 (likelihood ratio chi-squared) and the LogWorth value calculated as –log10(*p*-value).

who concluded that SE was an accurate measure of Flowability of milled TPU with fine particles, these results suggest that the powder's ability to fluidise, as measured by the Aeration Test are a more accurate measure of Flowability during the spreading of the milled PAEK samples. The investigation of Snow et al., [22] also concluded that SE and FRI demonstrated no significant link with spreadability. The circularity was not found to have significant influence on the spreading response, whereas Van den Eynde et al., [4] found the PS monodisperse spheres spread a smooth layer on their self-built powder spreading rig. This may be due to the PAEK samples all being milled particles, where Van Den Eynde et al., were comparing spherical, rounded and milled particles. When considering the results in Table 3, the only exception to the prediction of NAS > 0.31 is the PEK sample which was found to fail the spreading trial even with a recorded NAS value of 0.40. This indicates that the Partition Model for this data set is not completely accurate. Alternative methods of prediction such as Artificial Neural Networks (ANN) [36] may provide a more accurate result. There is currently limited published research into the use of ANN's for the design of feedstock materials for PBF [37], whereas much of the research is focussed on the application of ANN's in the optimisation of PBF process parameters and their effect on part properties [36] or defect detection [38–40].

From the spreading trial results presented in Table 4 it was noted that the thermally treated samples which passed the spreading trial all recorded a higher CBD than their untreated variants (Table 3). The thermal treatment is not a value considered in the partition model, and although the increase in CBD after thermal treatment is a consistent trend, there is not a threshold value above which spreading is successful, unlike the NAS.

4. Conclusions

In this unique study, twenty-four milled PolyArylEtherKetone powders, which the authors believe to represent the largest published study of PAEK polymer powders for Additive Manufacturing, were used to identify correlations between flow parameters, particle size distribution and circularity – as a shape descriptor.

The Basic Flow Energy has been proven to be very strongly influenced by the Conditioned Bulk Density and the Compressibility, both of which values are very strongly linked with the mean circularity. The Normalised Aeration Sensitivity has a strong relationship with both the Conditioned Bulk Density and the Permeability identifying powders which fluidise easily form a denser and less permeable bulk solid. The pressure drop (PD) for the powders proven to spread, is higher than the pressure drop value of the untreated powders, indicating that less permeable powders (higher PD) are desirable for good spreading and the relationships between PD, FRI, NAS and D10 are proven to be strong. The Circularity is identified as influential on the CBD, BFE and the CPS indicating that more rounded particles result in improved packing. The correlation of the D10 with powder rheology data highlights that just monitoring D50 values in PSD (values which are mostly cited in additive manufacturing powder literature) is not sufficient to design suitable powders for additive manufacturing. The D10 value can be effectively modified through established methods such as milling and sieving.

The partition model highlighted that NAS is the only indicator for predicting spreadability for this selection of PAEK milled powders. A closer examination of the powders with NAS values >0.31 s/mm showed that those successfully spreading are thermally treated and had increased CBD over their untreated counterparts.

It is desirable in the development of polymer powders suitable for powder bed fusion to be able to characterise and predict powder performance from reduced material batch sizes and without the significant investment in PBF systems. By fully understanding the relationships of data gathered from analytical equipment common to powder analysis and using established statistical techniques the cost and time of developing new materials for additive manufacturing can be reduced.

CRediT authorship contribution statement

Richard Davies: Conceptualization, Methodology, Writing – original draft, Formal analysis, Writing – review & editing. **Ken Evans:** Writing – review & editing, Supervision. **Oana Ghita:** Conceptualization, Writing – review & editing, Supervision.

Declaration of Competing Interest

The authors declare that they have no known competing financial interests or personal relationships that could have appeared to influence the work reported in this paper.

Data availability

Data will be made available on request.

Acknowledgements

The authors would like to thank Victrex Plc for their support and for supplying the materials used in this study.

Appendix A

Table 6
Multivariate Correlation values of powder rheometer, particle size distribution and circularity average value relationships.

	BFE, mJ	SI	FRI	SE, mJ/g	CBD, g/ml	CPS, %	PD, mBar	AE_10, mJ	AR_10, mJ	NAS, s/mm	D90	D50	D10	PSD Span	Circularity
BFE, mJ	1.000	0.134	−0.313	0.535	0.890	−0.837	−0.064	−0.059	0.527	0.499	−0.399	−0.304	0.387	−0.328	0.598
SI	0.134	1.000	−0.283	−0.143	−0.035	0.065	−0.036	−0.408	0.347	0.378	−0.308	0.108	0.245	−0.366	−0.186
FRI	−0.313	−0.283	1.000	−0.097	0.020	0.033	0.754	−0.109	−0.208	0.352	0.197	−0.434	−0.787	0.472	0.190

(*continued on next page*)

Table 6 (*continued*)

	BFE, mJ	SI	FRI	SE, mJ/g	CBD, g/ml	CPS, %	PD, mBar	AE_10, mJ	AR_10, mJ	NAS, s/mm	D90	D50	D10	PSD Span	Circularity
SE, mJ/g	0.535	−0.143	−0.097	1.000	0.495	−0.327	0.010	0.280	0.123	0.081	0.033	−0.517	0.070	0.230	0.548
CBD, g/ml	0.890	−0.035	0.020	0.495	1.000	−0.905	0.319	−0.182	0.493	0.641	−0.325	−0.562	0.028	−0.105	0.805
CPS, %	−0.837	0.065	0.033	−0.327	−0.905	1.000	−0.161	0.183	−0.456	−0.570	0.302	0.387	−0.133	0.165	−0.759
PD, mBar	−0.064	−0.036	0.754	0.010	0.319	−0.161	1.000	−0.426	0.108	0.619	0.019	−0.590	−0.785	0.350	0.416
AE_10, mJ	−0.059	−0.408	−0.109	0.280	−0.182	0.183	−0.426	1.000	−0.752	−0.589	0.338	0.211	0.121	0.237	−0.168
AR_10, mJ	0.527	0.347	−0.208	0.123	0.493	−0.456	0.108	−0.752	1.000	0.467	−0.391	−0.179	0.303	−0.361	0.310
NAS, s/mm	0.499	0.378	0.352	0.081	0.641	−0.570	0.619	−0.589	0.467	1.000	−0.270	−0.426	−0.253	−0.069	0.475
D90	−0.399	−0.308	0.197	0.033	−0.325	0.302	0.019	0.338	−0.391	−0.270	1.000	0.346	−0.244	0.876	−0.267
D50	−0.304	0.108	−0.434	−0.517	−0.562	0.387	−0.590	0.211	−0.179	−0.426	0.346	1.000	0.480	−0.137	−0.725
D10	0.387	0.245	−0.787	0.070	0.028	−0.133	−0.785	0.121	0.303	−0.253	−0.244	0.480	1.000	−0.563	−0.134
PSD Span	−0.328	−0.366	0.472	0.230	−0.105	0.165	0.350	0.237	−0.361	−0.069	0.876	−0.137	−0.563	1.000	0.044
Circularity	0.598	−0.186	0.190	0.548	0.805	−0.759	0.416	−0.168	0.310	0.475	−0.267	−0.725	−0.134	0.044	1.000

References

[1] J.W. Stansbury, M.J. Idacavage, 3D printing with polymers: challenges among expanding options and opportunities, in: Dental Materials, Elsevier Inc., 2016, pp. 54–64, https://doi.org/10.1016/j.dental.2015.09.018.

[2] D. Bourell, J.P. Kruth, M. Leu, G. Levy, D. Rosen, A.M. Beese, A. Clare, Materials for additive manufacturing, CIRP Ann. 66 (2017) 659–681, https://doi.org/10.1016/J.CIRP.2017.05.009.

[3] M. Schmid, R. Kleijnen, M. Vetterli, K. Wegener, Influence of the origin of polyamide 12 powder on the laser sintering process and laser sintered parts, Appl. Sci. (Switzerland). 7 (2017), https://doi.org/10.3390/app7050462.

[4] M. van den Eynde, L. Verbelen, P. van Puyvelde, Assessing polymer powder flow for the application of laser sintering, Powder Technol. 286 (2015) 151–155, https://doi.org/10.1016/j.powtec.2015.08.004.

[5] Z. Zeng, X. Deng, J. Cui, H. Jiang, S. Yan, B. Peng, Improvement on selective laser sintering and post-processing of polystyrene, Polymers (Basel). 11 (2019), https://doi.org/10.3390/polym11060956.

[6] G. Wang, P. Wang, Z. Zhen, W. Zhang, J. Ji, Preparation of PA12 microspheres with tunable morphology and size for use in SLS processing, Mater. Des. 87 (2015) 656–662, https://doi.org/10.1016/j.matdes.2015.08.083.

[7] M.S. Wahab, K.W. Dalgarno, R.F. Cochrane, Selective laser sintering of polymer nanocomposites, in: International Solid Freeform Fabrication Symposium, Austin, 2007. http://utw10945.utweb.utexas.edu/Manuscripts/2007/2007-30-Wahab.pdf. (Accessed 9 June 2022).

[8] Y. Wang, J. Shen, M. Yan, X. Tian, Poly ether ether ketone and its composite powder prepared by thermally induced phase separation for high temperature selective laser sintering, Mater. Des. 201 (2021), https://doi.org/10.1016/j.matdes.2021.109510.

[9] B. Chen, B. Yazdani, L. Benedetti, H. Chang, Y. Zhu, O. Ghita, Fabrication of nanocomposite powders with a core-shell structure, Compos. Sci. Technol. 170 (2019) 116–127, https://doi.org/10.1016/j.compscitech.2018.11.046.

[10] S. Berretta, O. Ghita, K.E. Evans, Morphology of polymeric powders in Laser Sintering (LS): from polyamide to new PEEK powders, Eur. Polym. J. 59 (2014) 218–229, https://doi.org/10.1016/J.EURPOLYMJ.2014.08.004.

[11] B. Chen, Y. Wang, S. Berretta, O. Ghita, Poly Aryl Ether Ketones (PAEKs) and carbon-reinforced PAEK powders for laser sintering, J. Mater. Sci. 52 (2017) 6004–6019, https://doi.org/10.1007/s10853-017-0840-0.

[12] D. Schulze, Discussion of testers and test procedures, in: Powders and Bulk Solids, Behaviour, Characterization, Storage and Flow, 2007, pp. 162–198.

[13] J. Schwedes, Review on testers for measuring flow properties of bulk solids, Granul. Matter 5 (2003) 1–43, https://doi.org/10.1007/s10035-002-0124-4.

[14] M. Leturia, M. Benali, S. Lagarde, I. Ronga, K. Saleh, Characterization of flow properties of cohesive powders: a comparative study of traditional and new testing methods, Powder Technol. 253 (2014) 406–423, https://doi.org/10.1016/j.powtec.2013.11.045.

[15] J.Y.S. Tay, C.V. Liew, P.W.S. Heng, Powder flow testing: judicious choice of test methods, AAPS PharmSciTech 18 (2017) 1843–1854, https://doi.org/10.1208/s12249-016-0655-3.

[16] B. Yazdani, B. Chen, L. Benedetti, R. Davies, O. Ghita, Y. Zhu, A new method to prepare composite powders customized for high temperature laser sintering, Compos. Sci. Technol. 167 (2018) 243–250, https://doi.org/10.1016/j.compscitech.2018.08.006.

[17] Freeman Technology, FT4 Powder Rheometer Flow Tester. https://www.freemantech.co.uk/powder-testing/ft4-powder-rheometer-powder-flow-tester, 2022. (Accessed 16 May 2022).

[18] B. Chen, R. Davies, Y. Liu, N. Yi, D. Qiang, Y. Zhu, O. Ghita, Laser sintering of graphene nanoplatelets encapsulated polyamide powders, Addi. Manuf. 35 (2020), https://doi.org/10.1016/j.addma.2020.101363.

[19] B. Chen, S. Berretta, R. Davies, O. Ghita, Characterisation of carbon fibre (Cf) - Poly Ether Ketone (PEK) composite powders for laser sintering, Polym. Test. 76 (2019) 65–72, https://doi.org/10.1016/J.POLYMERTESTING.2019.03.011.

[20] Y. Tan, J. Zhang, X. Li, Y. Xu, C.Y. Wu, Comprehensive evaluation of powder flowability for additive manufacturing using principal component analysis, Powder Technol. 393 (2021) 154–164, https://doi.org/10.1016/j.powtec.2021.07.069.

[21] S. Ziegelmeier, F. Wöllecke, C. Tuck, R. Goodridge, R. Hague, Characterizing the bulk & flow behaviour of LS polymer powders, in: International Solid Freeform Fabrication Symposium, University of Austin at Texas, Austin, 2013, https://doi.org/10.26153/tsw/15437.

[22] Z. Snow, R. Martukanitz, S. Joshi, On the development of powder spreadability metrics and feedstock requirements for powder bed fusion additive manufacturing, Addi. Manuf. 28 (2019) 78–86, https://doi.org/10.1016/j.addma.2019.04.017.

[23] Y. Jin, N. Chen, Y. Li, Q. Wang, The selective laser sintering of a polyamide 11/BaTiO3/graphene ternary piezoelectric nanocomposite, RSC Adv. 10 (2020) 20405–20413, https://doi.org/10.1039/d0ra01042a.

[24] Victrex Plc, https://www.victrex.com/en/products/polymers/peek-polymers. https://www.victrex.com/en/products/polymers/peek-polymers, 2022. (Accessed 16 May 2022).

[25] F. Muller, A. Pfister, M. Leuterer, PAEK Powder, Particularly for Use in a Method for the Production of a Three-Dimensional Object in Layers, and Method for the Production Thereof, EP2115043B1, 2008.

[26] Microtrac, Microtrac Sync - Particle Size Shape Analysis. https://www.microtrac.com/products/particle-size-shape-analysis/laser-diffraction/sync/, 2022. (Accessed 10 June 2022).

[27] Microtrac, Particle Size shape analysis, laser diffraction, sync. https://www.microtrac.com/products/particle-size-shape-analysis/laser-diffraction/, 2022. (Accessed 10 June 2022).

[28] Freeman Technology, Dynamic Energy Calculation, 2017.

[29] SAS Insitute Inc, JMP Documentation Library, Cary, NC, 2019.

[30] S. Berretta, K.E. Evans, O. Ghita, Processability of PEEK, a new polymer for high temperature laser sintering (HT-LS), Eur. Polym. J. 68 (2015) 243–266, https://doi.org/10.1016/J.EURPOLYMJ.2015.04.003.

[31] M. van den Eynde, L. Verbelen, P. van Puyvelde, Influence of temperature on the flowability of polymer powders in laser sintering, in: AIP Conference Proceedings, American Institute of Physics Inc., 2017, https://doi.org/10.1063/1.5016796.

[32] I. Tomasetta, D. Barletta, M. Poletto, The High Temperature Annular Shear Cell: a modified ring shear tester to measure the flow properties of powders at high temperature, Adv. Powder Technol. 24 (2013) 609–617, https://doi.org/10.1016/j.apt.2012.11.007.

[33] D. Ruggi, C. Barrès, J.Y. Charmeau, R. Fulchiron, D. Barletta, M. Poletto, A quantitative approach to assess high temperature flow properties of a PA 12 powder for laser sintering, Addi. Manuf. 33 (2020), 101143, https://doi.org/10.1016/J.ADDMA.2020.101143.

[34] Anton Paar, Anton Paar Modular Compact Rheometer. https://www.anton-paar.com/uk-en/products/details/rheometer-mcr-702-multidrive/, 2022. (Accessed 17 June 2022).

[35] J.D. Evans, Straightforward Statistics for the Behavioral Sciences, Brooks/Cole Publishing Company, 1996.

[36] R.-J. Wang, J. Li, F. Wang, X. Li, Q. Wu, ANN Model for the Prediction of Density in Selective Laser Sintering, 2009.

[37] W. Zhang, A. Mehta, P.S. Desai, C. Fred Higgs III, Machine learning enabled powder spreading process map for metal additive manufacturing (AM), in: International Solid Freeform Fabrication Symposium, Austin, 2017.

[38] L. Scime, J. Beuth, A multi-scale convolutional neural network for autonomous anomaly detection and classification in a laser powder bed fusion additive manufacturing process, Addi. Manuf. 24 (2018) 273–286, https://doi.org/10.1016/j.addma.2018.09.034.

[39] L. Scime, J. Beuth, Using machine learning to identify in-situ melt pool signatures indicative of flaw formation in a laser powder bed fusion additive manufacturing process, Addi. Manuf. 25 (2019) 151–165, https://doi.org/10.1016/j.addma.2018.11.010.

[40] E. Westphal, H. Seitz, A machine learning method for defect detection and visualization in selective laser sintering based on convolutional neural networks, Addi. Manuf. 41 (2021), https://doi.org/10.1016/j.addma.2021.101965.